J. Opt. B: Quantum Semiclass. Opt. **2** (2000) 399–405. Printed in the UK PII: S1464-4266(00)09631-2

Localized versus delocalized patterns in a nonlinear optical interferometer

P L Ramazza†, S Ducci†‡, S Boccaletti†§ and F T Arecchi†‡

† Istituto Nazionale di Ottica, I50125 Florence, Italy and INFM Sezione di Firenze, Italy
‡ Department of Physics, University of Florence, I50125 Florence, Italy
§ Department of Physics and Applied Mathematics, Universidad de Navarra, 31080 Pamplona, Spain

Received 17 November 1999, in final form 28 February 2000

Abstract. We compare the morphology of the spatial structures displayed by an optical system consisting of a liquid crystal light valve (LCLV) in a feedback configuration, as the feedback is gradually tuned from purely diffractive to mixed interferential and diffractive. Different kinds of spatially coherent structures (e.g. hexagons, rolls), as well as localized structures and space–time turbulent patterns are observed. The features of the localized structures change with the parameter setting, and certain regions of the parameter space provide stable clusters of isolated spots ('molecules'). Numerical simulations based on a Kerr-like model of the LCLV are in agreement with the experimental observations. We analyse the links between the observed behaviours and the results of a linear-stability analysis of the underlying homogeneous stationary states.

Keywords: Nonlinear optics, pattern formation, liquid crystal light valve

1. Introduction

Pattern formation in spatially extended systems driven out of thermal equilibrium is a widespread phenomenon in nature, and has been extensively studied in recent years [1]. In this regard, nonlinear optics represents a fruitful area of investigation, since several nonlinear optical systems display bifurcations to patterned states [2–4]. Among these systems, the slice of Kerr material enclosed in a feedback loop and exposed to a uniform input beam is one of the most studied [5–10]. The fact that the optical nonlinearity and the diffractive propagation occur in spatially separated regions yields a relatively simple theoretical model of this system; in addition, the existence of hybrid electro-optical devices working with liquid crystals (LCs) allows one to have large nonlinearities at low input intensities, and consequently to study systems with large aspect ratios. A large variety of morphologies occurring in such a system have been investigated both theoretically and experimentally. Among these, we recall hexagons [11] and states of spatotemporal chaos [12] for a purely diffractive feedback, and localized structures [13, 14] when the feedback is both interferential and diffractive.

In this paper we present a systematic study of the state diagram of a system composed of a liquid crystal light valve (LCLV) with feedback, in a two-dimensional parameter space. The chosen parameters are the input intensity and a geometric parameter of the system characterizing the ratio of interferential to diffractive contributions in the feedback loop. Our work may be considered as complementary to a previous study on the same system [13]; a comparison of the different parameter settings is left to the conclusions section.

The investigation reported is both experimental and numerical. Numerical simulations are based on a Kerr-like model of the LCLV, that is shown to describe with good accuracy the device nonlinearity for the input-intensity levels used in the experiment. In some regions of the parameter space, a linear-stability analysis of the model is useful to understand the behaviour of the system even in situations where the bifurcated signals do not have small amplitude. For other regions, the information given by the linear-stability analysis is not easily correlated with the behaviours observed in the nonlinear regime. We identify the regions of existence and stability of several kinds of spatial structures. In particular, in a broad region of the parameter space localized structures are present, giving rise in some cases to molecule-like aggregations.

2. Model of the experiment and linear-stability analysis

The experimental setup we use is shown in figure 1(*a*). It consists of a LCLV inserted into an optical feedback loop. The LCLV is formed by a nematic LC cell, followed by a mirror and a layer of photoconductive material [15]. A voltage of rms amplitude V_0 at frequency ν is applied to the series of these three elements. The fraction V_{LC} of this voltage across the LC cell is determined both by V_0 and ν, and by the light intensity I_W (writing intensity) impinging on the photoconductive layer. Due to V_{LC}, the nematics LC reorient, thus inducing a phase retardation on an input beam traversing the cell (actually, there is a double passage of the

1464-4266/00/030399+07$30.00

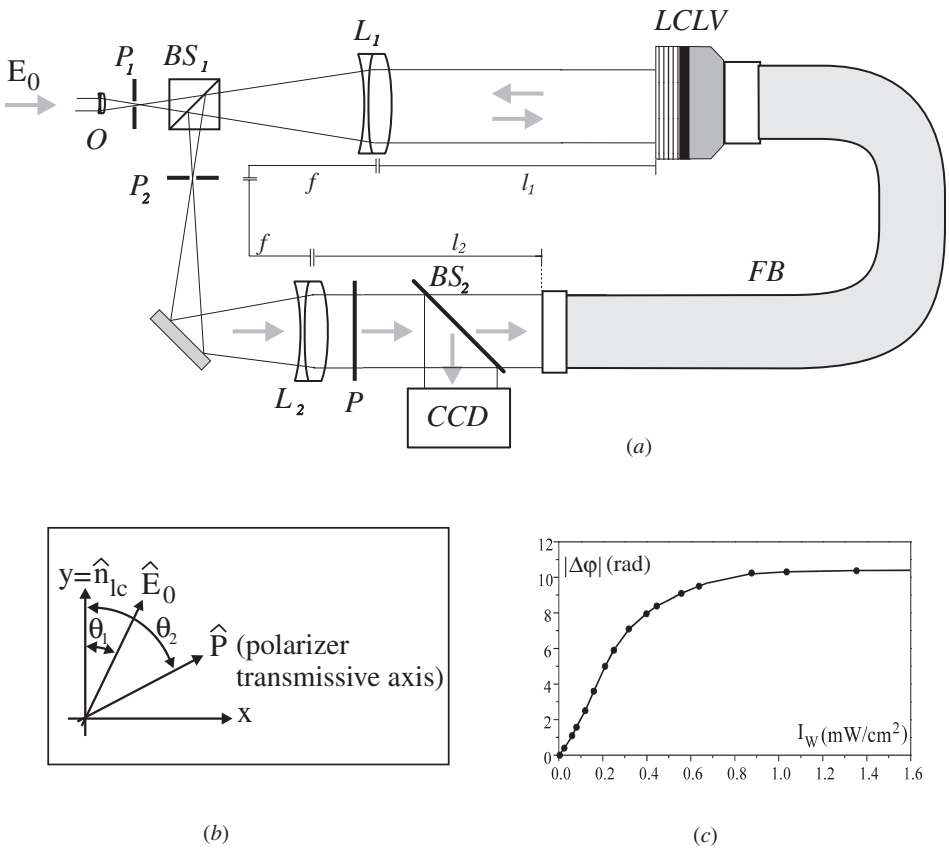

Figure 1. (*a*): Experimental setup. E_0 = input field; O = microscope objective; P_1, P_2 = pinholes; BS_1, BS_2 = beam splitters; LCLV = liquid crystal light valve; L_1, L_2 = lenses of focal length f; P = polarizer; FB = fibre bundle; CCD = videocamera. (*b*) Scheme explaining the definition of the angles θ_1 and θ_2 used in the coefficients B and C. (*c*) Characteristic $|\Delta\varphi|$ versus I_W curve of the valve for $V_0 = 8$ V, $\nu = 2.5$ KHz.

beam through the LC because the mirror reflects it back). In a certain range of the parameter values, this phase retardation is proportional to I_W, so that, using a closed-loop configuration, the LCLV behaves like a Kerr medium.

If small perturbations in the spatial distribution of the LC orientation (and hence of the optical phase induced in the input beam) are subject to a strong positive feedback, the system can give rise to pattern-forming instabilities. Since, however, the feedback is sensitive to intensity rather than to phase distributions, destabilization of the uniform states of the system requires a mechanism of transformation of phase into intensity modulations. This mechanism is due to either diffractive-free propagation [6], or to interference between the input beam and a reference beam [8, 13, 16]. In this paper, both mechanisms are explored. In particular, a propagation over an effective negative length is obtained by a proper choice of the distances l_1 between lens L_1 and the front face of the LCLV, and l_2 between lens L_2 and the rear face of the LCLV. In these conditions the nonlinearity of the overall system is of self-focusing type [13, 17], even if the intrinsic LCLV nonlinearity is self-defocusing. Then the components of the light polarized respectively parallel and perpendicular to the LC director interfere by means of the polarizer P inserted in the feedback loop [13]. In this way the electric field parallel to the LC director, that carries the phase information relevant to the system dynamics, is superimposed in the feedback loop to the constant-amplitude, constant-phase electric field perpendicular to the LC director. The equation governing the evolution of the phase φ induced by the LC cell on the input beam is

$$\tau \frac{\partial \varphi(\vec{r},t)}{\partial t} = -(\varphi(\vec{r},t) - \varphi_0) + l_d^2 \nabla_\perp^2 \varphi(\vec{r},t) + \alpha I_{fb}, \quad (1)$$

where $\varphi_0 = \varphi_0(V_0, \nu)$ is the constant-phase retardation induced by the LCLV in the absence of writing light on its back, l_d is a diffusion length and α gives the sign and strength of the Kerr nonlinearity. In the presence of a negative propagation length in the system, we have $\alpha > 0$. The feedback intensity $I_{\rm fb}$ is given by the expression [13]

$$I_{\rm fb} = I_0 |\mathrm{e}^{\frac{-il\nabla^2}{2k_0}}(B\mathrm{e}^{-\mathrm{i}\varphi} + C)|^2 = B^2 \mathrm{e}^{\frac{-il\nabla^2}{2k_0}} \mathrm{e}^{-\mathrm{i}\varphi} \mathrm{e}^{\frac{il\nabla^2}{2k_0}} \mathrm{e}^{\mathrm{i}\varphi} + BC(\mathrm{e}^{\frac{-il\nabla^2}{2k_0}} \mathrm{e}^{-\mathrm{i}\varphi} + \mathrm{e}^{\frac{+il\nabla^2}{2k_0}} \mathrm{e}^{\mathrm{i}\varphi}) + C^2. \quad (2)$$

Here I_0 is the input intensity, l is the free propagation length, $k_0 \equiv 2\pi/\lambda$ is the optical wavenumber, and B and C are given by

$$B = \cos\theta_1 \cos\theta_2 \qquad C = \sin\theta_1 \sin\theta_2, \quad (3)$$

θ_1 and θ_2 being respectively, the angles formed by the directions of the input light polarization and the polarizer P transmissive axis with the LC director (see figure 1(*b*)). From equation (2) it is seen that the feedback intensity is the sum of three contributions. The term C^2 only affects

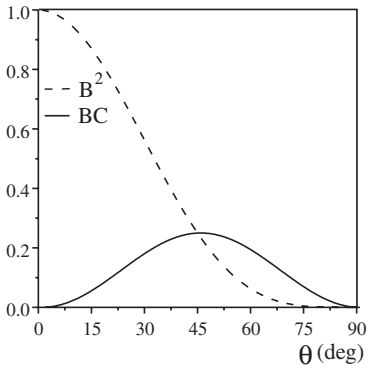

Figure 2. Plot of the coefficients B^2 (dashed curve) and BC (solid curve) versus θ. The diffractive contribution B^2 dominates at low values of θ, while the interferential contribution BC has a maximum weight at $\theta = 45^\circ$.

the dynamics of the uniform states. The terms in B^2 and BC weigh, respectively, the roles of diffraction and interference in determining the spatial distribution of $I_{\rm fb}$, and affect the dynamics of the nonuniform states leading to pattern formation. In figure 2 we plot B^2 and BC versus θ ($\theta \equiv \theta_1 = \theta_2$ is assumed here). It is seen that the diffractive contribution is dominant at low values of θ, while the interference has a maximum weight at $\theta = 45^\circ$. For very large θ values both terms become very small, because most of the light is absorbed by the polarizer.

In equation (1) we used the Kerr approximation, i.e. induced phase proportional to the writing intensity. A detailed analysis of the LCLV behaviour [13] has pointed out the limits of this approximation. In general, it is not valid at low light intensity and applied voltage V_0 because the LC molecules remain anchored to the cell walls at their equilibrium position, nor at high light intensity or voltage V_0 due to the saturation of the molecule reorientation.

In figure 1(c) we show the characteristic $|\Delta\varphi|$ versus I_W curve of our valve for the values $V_0 = 8$ V, $\nu = 2.5$ kHz that were fixed throughout the experiments reported here. It can be seen that the Kerr model describes adequately the behaviour of the device up to $I_W \simeq 0.4$ mW cm^{-2}, with a value of the constant $\alpha = 24 \pm 2$ cm^2 mW^{-1}.

In the following we specialize our analysis and experiment to the case in which $\theta_1 = \theta_2$. This choice is dictated by the necessity of limiting the number of relevant parameters, especially for the theoretical and numerical analysis of the system. Experimental observations for many values of θ_1, θ_2 with $\theta_1 \neq \theta_2$ have shown that most of the important behaviours of the system are already captured when choosing $\theta_1 = \theta_2 = \theta$ and varying θ. Another parameter we keep fixed is the value of the phase φ_0 induced by the LCLV on the input beam in the absence of writing light. This value is determined by the amplitude V_0 and the frequency ν of the voltage applied to the LCLV. The above-specified values were chosen so that $\varphi_0 = \pi$. This value was held fixed since it has proved experimentally convenient for the formation of many intensity patterns, first of all localized structures. At variance with what we said for θ_1 and θ_2, the system behaviour is highly sensitive to the value of φ_0. Indeed, φ_0 fixes the working point of the LCLV, and is equivalent to the 'bias intensity' J_b introduced in [13].

The parameters we vary in a systematic way are then the input intensity I_0, and the angle θ. We note that the feedback intensity equation (2) is invariant for the transformations $\theta \to \theta'$ that leave unchanged the values of B^2, C^2 and BC. A simple trigonometric analysis shows that this allows us to restrict the values of θ in the range $[0, \pi/2]$, since starting from these values all the possible angle between 0 and 2π are spanned by means of the variable changes $\theta' = \pi - \theta$, $\theta'' = -\theta$, $\theta''' = \theta - \pi$, that leave the equation invariant.

Equation (1) with the feedback intensity given in equation (2) has the stationary homogeneous solution

$$\varphi^{(0)} = \varphi_0 + \alpha I_0(B^2 + C^2 + 2BC\cos\varphi^{(0)}). \qquad (4)$$

As we scan φ_0 the solutions are the multiple intersections of a straight line (left-hand side) with the trigonometric function on the right-hand side. The number of possible solutions depends on the coefficient αI_0. In the following we limit the input intensity I_0 to values of $\alpha I_0 \lesssim 7$ (that is $I_0 \lesssim 0.3$ mW cm^{-2}), so that only the first three branches of stability (two stable and one unstable) have to be considered for each value of θ. We limit this range because for $\alpha I_0 \gtrsim 7$ the Kerr description of the LCLV nonlinearity is no more valid and hence the same nature of the homogeneous stationary solutions is different from that expressed by equation (4). If we now perform a linear stability analysis of equation (1) around the solutions of equation (4) by letting

$$\varphi(\vec{r}, t) = \varphi^{(0)} + \varphi(q)\mathrm{e}^{\mathrm{i}q\vec{r}}\mathrm{e}^{\lambda t}, \qquad (5)$$

we evaluate the following growth rate λ for the spatial-frequency mode q:

$$\tau\lambda(q) = -(1 + l_d^2 q^2) + 2\alpha I_0[2B^2\sin(q^2 l/2k_0) + 2BC\sin(q^2 l/2k_0 - \varphi^{(0)})]. \qquad (6)$$

It is soon recognized that if the interference term $2BC$ is absent, as it occurs (figure 2) for $\theta = 0$, equation (6) gives the well-known expression for the eigenvalues of the purely diffractive problem [6]. This results in the selection of a maximally unstable mode at a spatial frequency $q_c = \sqrt{\pi k_0/l}$, in the limit of small diffusion $l_d q_c \ll 1$, as it occurs in the experiment. Conversely, if diffraction is absent ($B = 0$), it is clear that the lack of destabilizing terms in (6) leads to the impossibility of pattern formation. From the expression of the eigenvalues it is to be expected that the introduction of interference in an otherwise purely diffractive configuration will lead to variations in both the most unstable wavenumber and in the value of I_0 for which this wavenumber is destabilized.

The marginal stability curves $\lambda(q) = 0$ in the plane $(\bar{q}^2, \varphi)$ are shown in figure 3, together with the corresponding solution for the homogeneous stationary phase $\varphi^{(0)}$ versus αI_0. Here $\bar{q}$ denotes a spatial frequency normalized to q_c. We recall that the portion of the stability balloons at $\bar{q}^2 < 0$ are physically meaningless, though we display a small part of them in order to give a better insight of the evolution of these curves as θ is varied.

From figure 3 it can be seen that for low values of θ the effect of the introduction of interference consists mainly in a bending of the stability balloons toward low frequencies and in a slight increase of the threshold. At $\theta \simeq 31^\circ$ the stability balloon touches the $q = 0$ axis. This corresponds to the fact,

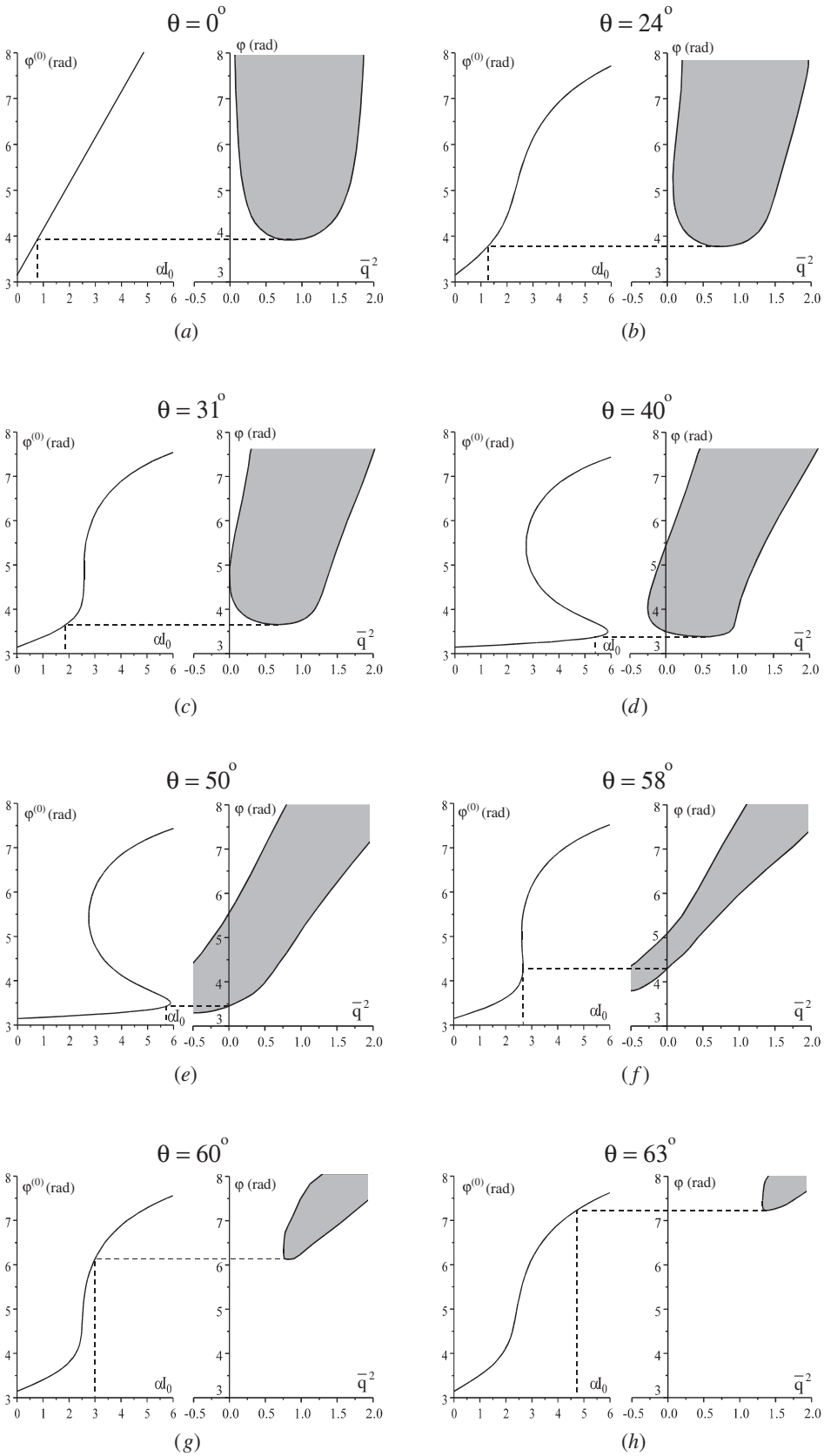

Figure 3. Marginal stability curves $\lambda(q) = 0$ in the plane $(\bar{q}^2, \varphi)$ together with the corresponding solutions for the homogeneous stationary phase $\varphi^{(0)}$ versus I_0 for different values of the angle θ. $\bar{q}$ is the spatial frequency normalized to q_c. Throughout all the simulations, the diffusion length l_d was kept fixed at 23 μm.

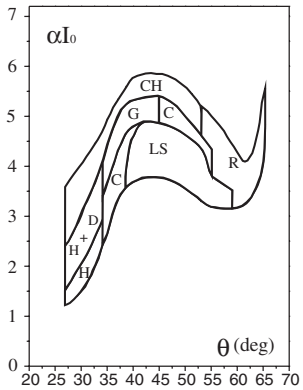

Figure 4. Experimental state diagram showing the types of patterns observed in the $(\alpha I_0, \theta)$ plane: H = hexagons; H + D = hexagons with defects; CH = chaos; LS = localized structures; C = collection of localized structures; G = gears; R = rolls.

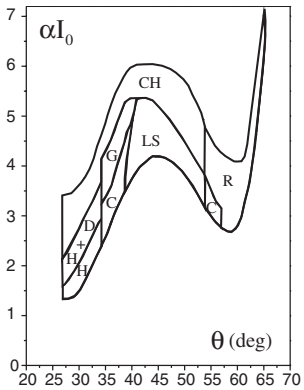

Figure 5. State diagram obtained from numerical simulations corresponding to the experimental one reported in figure 4; the symbols have the same meaning as they have in figure 4.

observable in the $\varphi^{(0)}$ versus I_0 curve, that bistability of the homogeneous solution arises. For $31^\circ \lesssim \theta \lesssim 45^\circ$ the lower branch of the φ^0 versus I_0 curve displays an instability at a finite wavenumber, while the upper branch is unstable with respect to a whole band of spatial frequencies. An example of this is shown in figure 3(d). In figure 3(e) we plot the stationary solution φ^0 and its stability balloon for $\theta = 50^\circ$. In this case the lower branch of the solution is stable with respect to finite-wavenumber perturbations, while the upper branch is unstable. A similar situation occurs in the range $45^\circ \lesssim \theta \lesssim 59^\circ$.

The behaviour described here is qualitatively analogous to the one reported in a model of a nonlinear interferometer filled with a Kerr medium described in the mean field approximation [18]. For $\theta > 50^\circ$ the stability balloon is displaced at higher frequencies and higher values of threshold intensity. At $\theta = 59^\circ$ the bistability of the homogeneous state disappears, and at higher values of θ the system displays instability toward a single finite spatial frequency. At variance with the situation observed for $\theta < 31^\circ$, however, now the selected wavenumber and threshold level depend strongly on θ. In particular, the threshold increase for $\theta > 65^\circ$ does not allow us to make experimental observations consistent with the Kerr description of the LCLV that we assume here.

3. Experimental results and numerical simulations

Both in the experiment and in the numerical simulations, we let θ vary between 25° and 65°. For smaller values of θ the system displays a behaviour very similar to the purely diffractive one. For larger values of θ, the threshold intensities are so high that it is very difficult to observe the patterns, that anyway would not be described in the framework of the Kerr description of the LCLV nonlinearity.

Experiments and simulations give clear indication that a crucial parameter for pattern selection is the spatial Fourier bandwidth of the system. Since we have free access to this parameter by means of the pinhole P_2 put in the common focal plane of the lenses Ł$_1$ and L_2, we have actually one more parameter to set. In both the experiment and simulations, we fixed an upper frequency cutoff at $q_{\max} = 1.8q_c$. In this way only the first two unstable bands, that in the purely diffractive limit are centred at $q_c = 1$ and $q_c = \sqrt{3}$, participate at the dynamics. The band around $q_c = \sqrt{3}$, however, only plays a relevant role in the space–time chaotic states observed at high-input intensities. We stress that changing this cutoff leads to strong quantitative, and in some cases also qualitative, variations in the observed phenomena.

Since we are dealing with a bistable and hence hysteretic system, the patterns observed depend not only on the intensity value set, but also on the history of the variations through which this value has been reached.

We basically have to choose if we make the observations as the control parameter, i.e. the input intensity I_0, is increased or decreased to a certain value. In many of the situations considered here, however, the lower branch is always stable and the upper one unstable with respect to a large band of wavenumbers. Hence, an increase of I_0 will result in no pattern formation until the turning point of the φ^0 versus I_0 curve is reached, followed by a jump of the system in the vicinity of the upper branch, where it displays a turbulent behaviour due to the excitation of the large unstable band. This kind of scenario is more distinct the more pronounced the S-shape of the bistabilty curves. Alternatively, when I_0 is decreased starting from a value for which the system is on the upper unstable branch down to a value for which even the lower branch is stable, both the level of excitation and the spatial unstable bandwidth are decreased. This gives rise to a sequence of distinct, well-recognizable behaviours. The experimental state diagram showing the kind of patterns observed in the $(\alpha I_0, \theta)$ plane is shown in figure 4. Its counterpart obtained from numerical simulations is presented in figure 5.

The experiment was carried out using an Ar^+ laser operating at 514 nm, with a propagation length $l = -150$ mm, resulting in a focusing nonlinearity of the system. Simulations have been performed using a pseudospectral method on a 128×128 point grid. The accuracy of the model can be seen by the synoptical comparison of the experimental frames, reported in figure 6, with the simulation frames, reported in figure 7.

For $\theta \leqslant 35^\circ$ the system forms hexagons at threshold. At higher I_0 values defects begin to form in the hexagonal texture, leading eventually to space–time chaotic situations. These behaviours are similar to the ones already reported

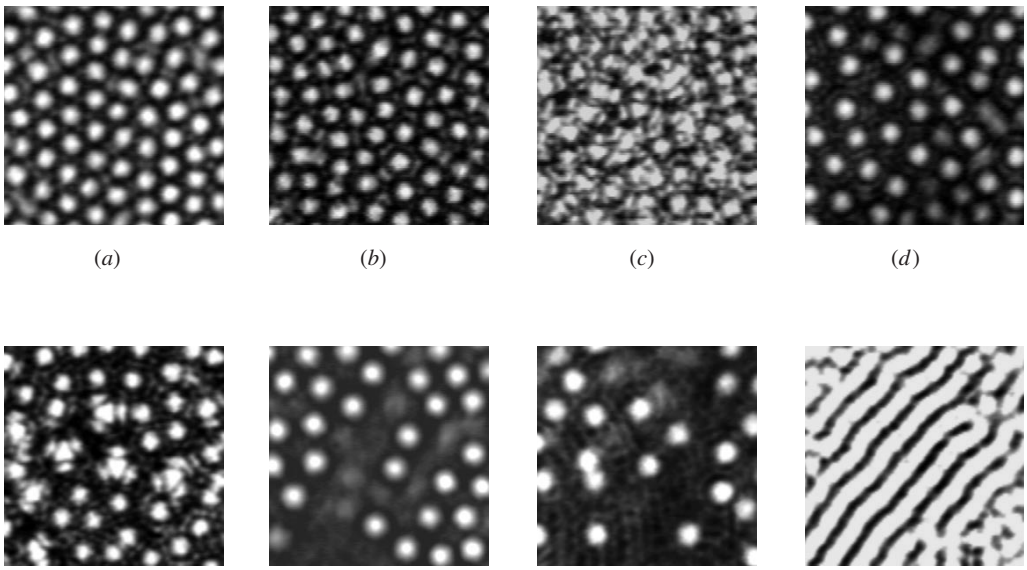

Figure 6. Experimental intensity distributions obtained for different points of the state diagram: (*a*) $\theta = 27^\circ$, $\alpha I_0 = 1.44$; (*b*) $\theta = 27^\circ$, $\alpha I_0 = 2.09$; (*c*) $\theta = 27^\circ$, $\alpha I_0 = 3.5$; (*d*) $\theta = 37^\circ$, $\alpha I_0 = 3.02$; (*e*) $\theta = 37^\circ$, $\alpha I_0 = 4.1$; (*f*) $\theta = 39^\circ$, $\alpha I_0 = 3.8$; (*g*) $\theta = 55^\circ$, $\alpha I_0 = 3.48$; (*h*) $\theta = 58^\circ$, $\alpha I_0 = 4.8$.

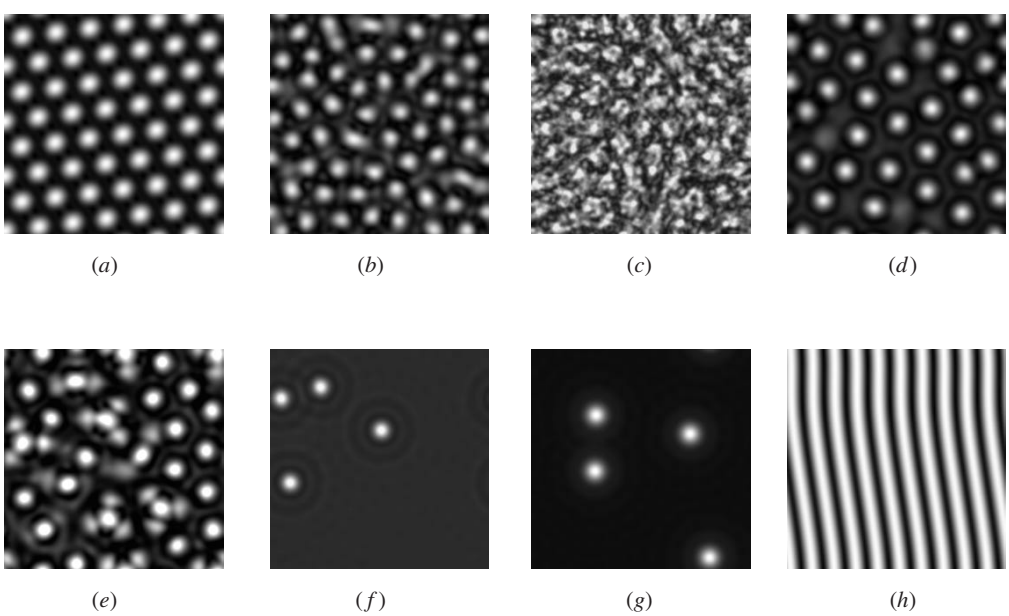

Figure 7. Intensity distribution obtained from numerical simulations for different points of the state diagram reported in figure 5: (*a*) $\theta = 27^\circ$, $\alpha I_0 = 1.5$; (*b*) $\theta = 27^\circ$, $\alpha I_0 = 2.00$; (*c*) $\theta = 27^\circ$, $\alpha I_0 = 3.20$; (*d*) $\theta = 37^\circ$, $\alpha I_0 = 2.80$; (*e*) $\theta = 37^\circ$, $\alpha I_0 = 4.00$; (*f*) $\theta = 41^\circ$, $\alpha I_0 = 4.10$; (*g*) $\theta = 55^\circ$, $\alpha I_0 = 3.30$; (*h*) $\theta = 63^\circ$, $\alpha I_0 = 4.80$.

in the purely diffractive system [6, 10], and their origin is reasonably retrieved from the observation of the marginal stability curves. A single scale is selected at threshold, and successive broadening of the excited band as I_0 is increased leads to more complicate dynamics. Bistability of the uniform states does not play an appearent role. Snapshots of typical patterns observed in these regimes are shown in figures 6(*a*)–(*c*) and 7(*a*)–(*c*).

In the range $35^\circ < \theta < 40^\circ$ the spots observed close to threshold are no longer packed in a regular hexagonal lattice, rather they form a collection of spatially uncorrelated localized structures (figures 6(*d*) and 7(*d*)). These collections are constituted by several spots without a spatial order; the distance between nearest-neighbour spots is of the order of their transverse size. At higher I_0 values, very regular clusters of four spots displaying a three-fold symmetry ('gears') are formed (figures 6(*e*) and 7(*e*)). We guess that this symmetry is related to the quadratic nonlinearity that in other regimes leads to hexagon formation, though an explanation of this molecule-like object formation is not yet available.

For $40^\circ < \theta < 55^\circ$ localized structures are observed in an intensity range that varies with θ. We argue that these

localized structures arise from the connection between the lower uniform state, which is stable over a broad range of parameters, and a coexisting patterned state. This kind of patterned state can be observed for the same values of the parameters at which localized structures occur, but reaching the working point through a different parameter history, e.g. by reaching the same parameter values by increasing rather than decreasing the input intensity. The amplitude of these delocalized patterns is very similar to that of the single localized spots. Preliminar observations have shown that the symmetry of these patterns is hexagonal for low values of θ, but not well defined for larger values, and that their scale does not depend on θ very much. This mechanism of localized structure formation is analogous to the one reported in other optical systems [19–21]. It is worth noting that the profile of the localized structures changes considerably for increasing values of θ (see figures 6(f), (g) and 7(f), (g) as examples); in particular the oscillatory tails, which are expected to play a stabilizing role [22], become less pronounced or even disappear for large θ values. Some qualitative differences are observed between the experimental and numerical state diagrams in this regime. First of all, these differences depend on the procedure used. The region boundaries in the experimental as well as in the numerical state diagram of figures 4 and 5 depend on the selected categorization criterion indicated by the symbols within each domain, criterion which may leave ambiguities at the domain edges. For this reason the boundaries are rather unsharp even though they have been drawn as lines. Furthermore, the region of existence of localized structures is narrower in the simulations than in the experiment. We believe that this is at least partly due to the choice of initial conditions in the simulations. Indeed, all the simulations start from a random spatial noise distribution, and for high I_0 the system is space–time chaotic in a uniform way. When I_0 is decreased, the situation remains turbulent until, in a short transient, the chaotic structure breaks, resulting in the appearence of few localized spots. This steep transition is smoothed by spatial inhomogeneities in the experimental case, in which we observe transitions from space–time chaos to collections of uncorrelated spots, and finally to isolated localized structures.

Finally, for $54^\circ < \theta < 65^\circ$ we observe roll formation in a broad range of input intensities (figures 6(h) and 7(h)). The scale selection and the increase of threshold intensity are well accounted for by the linear stability analysis. The symmetry of these patterns indicates that the quadratic nonlinearity is small or vanishing in this regime. Nonlinear stability analysis of the model equation has given results in agreement with these observations [23].

4. Conclusions

We have presented a systematic investigation of pattern formation in a nonlinear interferometer formed by a LCLV with feedback, when the system configuration is gradually tuned from purely diffractive to mixed diffractive–interferential.

Throughout all the measurements, the system parameters were kept at values for which the Kerr description of the LCLV nonlinearity holds. This constitutes a major difference with respect to the study presented in [13], where the influence of the initial and terminal feature of the LCLV characteristic, that is, the internal threshold for disanchoring the molecules at low intensities and the saturation in the reorientation of the molecules at high intensities, on the pattern selection were investigated in detail. Also, our choice of the control parameters is somewhat complementary to that in [13]. Indeed, here we systematically investigate the role of the input intensity, while the study in [13] was mainly devoted to the dependence of the patterns on the working point φ_0 of the LCLV ('bias intensity J_b' in the notation of [13]).

Regions of existence of several delocalized as well as localized kinds of spatial structures have been identified and quantitatively delimited. Numerical simulations based on a Kerr model for the LCLV nonlinearity have given results in agreement with the experiments.

Acknowledgments

This work has been partly supported by ECC Contract FMRX CT960010 and the 1999 Italy–Spain Integrated Action.

References

[1] Cross M and Hohenberg P C 1993 *Rev. Mod. Phys.* **65** 851
[2] Lugiato L A (ed) 1994 Nonlinear optical structures, patterns, chaos *Chaos Solitons Fractals* (Special Issue) **4**
[3] Neubecker R and Tschudi T (ed) 1999 Pattern formation in nonlinear optical systems *Chaos Solitons Fractals* (Special Issue) **10**
[4] Arecchi F T, Boccaletti S and Ramazza P L 1999 *Phys. Rep.* **318**
[5] Akhmanov S A, Vorontsov M A and Ivanov V Yu 1998 *JETP Lett.* **47** 707
[6] Firth W J 1990 *J. Mod. Opt.* **37** 151
D'Alessandro G and Firth W J 1991 *Phys. Rev. Lett.* **66** 2597
[7] Macdonald R and Eichler H J 1992 *Opt. Commun.* **89** 289
[8] Akhmanov S A *et al* 1992 *J. Opt. Soc. Am.* B **9** 78
[9] Ramazza P L, Pampaloni E, Residori S and Arecchi F T 1996 *Physica* D **96** 259
Ramazza P L, Boccaletti S, Ducci S and Arecchi F T 1999 *J. Nonlinear Opt. Phys. Mater.* **8** 235
[10] Thuering B, Neubecker R and Tschudi T 1993 *Opt. Commun.* **102** 111
[11] Pampaloni E, Residori S and Arecchi F T 1993 *Europhys. Lett.* **24** 647
Neubecker R, Thuering B and Tschudi T 1994 *Chaos Solitons Fractals* **4** 1307
[12] Cataldo F, Paparo D and Santamato E 1997 *Opt. Commun.* **143** 57
[13] Neubecker R, Oppo G L, Thuering B and Tschudi T 1995 *Phys. Rev.* A **52** 791
[14] Schreiber A, Thuering B, Kreuzer M and Tschudi T 1997 *Opt. Commun.* **136** 415
[15] Vorontsov M A, Kirakosyan M E and Larichev A V 1991 *Sov. J. Quantum Electron.* **21** 105
[16] Vorontsov M A and Karpov A Yu 1997 *J. Opt. Soc. Am.* B **14** 34
[17] Ciaramella E, Tamburrini M and Santamato E 1993 *Appl. Phys. Lett.* **63** 1604
[18] Geddes J B *et al* 1994 *Chaos, Solitons and Fractals* **4** 1261
[19] Tlidi M, Mandel P and Lefever R 1994 *Phys. Rev. Lett.* **73** 640
[20] Firth W J and Scroggie A J 1996 *Phys. Rev. Lett.* **76** 1623
[21] Lugiato L A, Spinelli L, Tissoni G and Brambilla M 1999 *J. Opt. B: Quantum Semiclass. Opt.* **1** 43
[22] Coullet P, Elphick C and Repaux D 1987 *Phys. Rev. Lett.* **58** 431
[23] Ramazza P L, Ducci S and Arecchi F T in preparation